doi.org/10.1002/batt.202000197

Special Collection

Electrochemical Performance and Mechanism of Calcium Metal-Organic Battery

Jan Bitenc,*[a] Antonio Scafuri,[a, b, c, d] Klemen Pirnat,[a] Matic Lozinšek,[b, e] Ivan Jerman,[a] Jože Grdadolnik,[a] Bernard Fraisse,[c] Romain Berthelot,[c, d, f] Lorenzo Stievano,[c, d, f] and Robert Dominko*[a, b, d]

The abundance of Ca, its low redox potential and high specific capacity make Ca metal batteries an attractive energy storage system for the future. A recent demonstration of room temperature calcium plating/stripping opened a new avenue of the development, but the performance of cathode materials is lagging far behind. Due to the nature of divalent cations, conversion and coordination electrochemical reactions show better performance compared to insertion. Herein, we demonstrate the use of the anthraquinone-based polymer as a cathode material for the Ca metal-organic battery. Electrochemical mechanism investigation confirms the reversible reduction of the carbonyl bond and coordination with Ca^{2+} cations in the discharged state, opening a pathway toward high energy density battery. Continued performance of a 2-electrode cell is strongly hampered by the overpotential increase caused by the Ca stripping process on the Ca metal anode stating the need for further development of Ca electrolytes. Ca metal-organic battery promises to achieve cells with gravimetric energy density on the practical level compared to the state-of-the-art Li-ion batteries.

1. Introduction

Currently, Li-ion batteries (LIBs) are dominating the market of battery technologies with their applications ranging from portable electronics, electric vehicles to stationary energy storage. Their high energy density, long cycle life, low self-discharge and versatility make them preferable over other state-of-the-art battery technologies. However, the ever-increasing demand for energy storage is raising concerns about the availability and sustainability of the materials used in Li-ion cell production.[1–3] Therefore, research groups are actively pursuing new battery technologies with a focus on sustainable materials which can deliver attractive electrochemical properties.[4] This is by far not trivial and requires a holistic approach focused on the integrated development of all the cell components (electrolyte, active materials, additives…). The most likely scenario is that no alternative technology will be able to replace LIBs in all applications, but adapted alternative systems will be created for specific applications, significantly lowering the demand on the limited raw materials used in LIBs.

Among the most intriguing alternative battery systems are multivalent-ion batteries, especially batteries based on Ca, Mg, and Al chemistries. These elements all belong among the ten most abundant ones in the Earth's crust.[5] Their application is particularly interesting due to the high volumetric and gravimetric energy densities of the metal anodes, and indications that these metals might be less prone to the dendrite formation than Li metal.[6,7] A possible downside of multivalent metals is their redox potential, which can be considerably higher than that of Li metal. If no change in the cathode potential is presumed, the expected cell voltage decrease of the metal anode battery cells is 1.4, 0.7, and 0.2 V when moving from Li to Al, Mg, and Ca metal anode, respectively. Whereas the difference in the redox potential is the most favorable for Ca metal, research on Ca metal batteries has been, until recently, hindered by the lack of suitable electrolytes. The main issue of Ca electrolytes is their electrochemical stability in contact with the Ca metal due to low redox potential of the metallic Ca and a tendency towards the decomposition of the electrolyte.[8] There are two main approaches to tackle this issue: (i) the formation of a passivation layer on the Ca metal permeable to Ca^{2+} ions by

[a] Dr. J. Bitenc, A. Scafuri, Dr. K. Pirnat, Dr. I. Jerman, Prof. Dr. J. Grdadolnik, Prof. Dr. R. Dominko
National Institute of Chemistry
Hajdrihova 19, 1000 Ljubljana, Slovenia
E-mail: jan.bitenc@ki.si
robert.dominko@ki.si
[b] A. Scafuri, Dr. M. Lozinšek, Prof. Dr. R. Dominko
Faculty for Chemistry and Chemical Technology
University of Ljubljana
Večna pot 113, 1000 Ljubljana, Slovenia
[c] A. Scafuri, Dr. B. Fraisse, Dr. R. Berthelot, Prof. Dr. L. Stievano
ICGM, Université de Montpellier
CNRS, 34090 Montpellier, France
[d] A. Scafuri, Dr. R. Berthelot, Prof. Dr. L. Stievano, Prof. Dr. R. Dominko
Alistore-European Research Institute
CNRS FR 3104, Hub de l'Energie
Rue Baudelocque, 80039 Amiens, France
[e] Dr. M. Lozinšek
Jožef Stefan Institute
Jamova 39, 1000 Ljubljana, Slovenia
[f] Dr. R. Berthelot, Prof. Dr. L. Stievano
Réseau sur le Stockage Electrochimique de l'Energie (RS2E)
CNRS, 80039 Amiens, France

Supporting information for this article is available on the WWW under https://doi.org/10.1002/batt.202000197

Special Collection An invited contribution to a joint Special Collection between ChemElectroChem and Batteries & Supercaps dedicated to research Beyond Lithium-Ion Batteries

limited decomposition of a metastable electrolyte, or (ii) use of electrolytes that do not form the passivating layer.[9]

Although Ca plating/stripping was attempted using $Ca(AlCl_4)_2$ in $SOCl_2$ already four decades ago, the corrosion of Ca metal was an evident problem, and only Ca stripping could be confirmed.[10] Later, Ca plating in this electrolyte was confirmed with very low efficiency, well-below 10% through the reaction of the deposited metal with water and analysis of alkaline impurities.[11] Significant progress was accomplished by the use of $Ca(BF_4)_2$ salt in the mixture of ethylene carbonate and propylene carbonate solvents, which enabled Ca plating/stripping with improved Coulombic efficiency. Although electrochemical performance at elevated temperatures makes it less practical for commercial use.[12] A breakthrough at ambient temperature was recently achieved using $Ca(BH_4)_2$ and $Ca[B(hfip)_4]_2$ ($[B(hfip)_4]^-$ – tetrakis(hexafluoroisopropyl)borate) dissolved in ethereal solvents.[13–15] Although these studies exemplified significant progress for application of Ca metal anodes, the Coulombic efficiency still needs to be increased, and the passivation process on the surface of Ca metal better understood. Only then the high volumetric (2073 mAh/cm^3) and gravimetric (1337 mAh/g) capacity of the Ca metal anode can be utilized in real cells.

Ca^{2+} ion is a unique cation: it is bivalent like Mg^{2+}, but its ionic radius is more similar to the Na^+, which could mean that Ca^{2+} ion exhibits similar site preference.[9] There were several attempts to intercalate Ca^{2+} in different inorganic phases, but the electrochemical performance has always been far from the full reversibility.[16–18] Hence, a radically different approach, *i.e.*, the use of organic cathode materials is proposed herein. Organic electrodes offer electrochemical activity with a multitude of cations with various sizes and charges.[19] Reversible electrochemical performance of organic moieties was already demonstrated in various metal-organic batteries, including Li, Na, K, Mg, Zn, and Al.[20–25] Organics can also be produced from sustainable materials and at lower synthesis temperatures, which should help lower the carbon footprint of battery production.[26] The possible degradation of organic batteries in aprotic electrolytes due to dissolution can be easily mitigated by polymerization of the redox-active monomers. Polymerization requires a molecular linker, which leads to the increase of the atomic mass per electroactive group, although low molecular weight linkers contribute to a decrease of energy density of only a few percent.[20]

There is a plethora of different organic electrode materials that can operate in different ways: through reduction and storage of cations (n-type), oxidation and storage of anions (p-type)%ek; or via both mechanisms, being able to get reduced and oxidized (bipolar) at the same time. N-type cathodes are the most practical counterpart material for metal anodes because only the storage of metal cations will allow operation in the lean electrolyte conditions inside real battery cells. Among such materials, conjugated carbonyl materials exhibit high capacity, good reversibility and long-term stability in several different metal-organic systems.[25,27,28] Anthraquinone-based materials often serve as the model compounds due to their availability, relatively straightforward polymerization and the fact that their redox potential fits well within the voltage stability window of most battery electrolytes. To the best of our knowledge, organic materials based on the conjugated organic carbonyl compounds have been tested exclusively in aqueous Ca electrolytes.[29,30] Here, poly(anthraquinonyl sulfide) (PAQS) was tested against a Ca metal anode using a state-of-the-art non-aqueous Ca electrolyte based on $Ca[B(hfip)_4]_2$ salt dissolved in DME (dimethoxyethane). Its electrochemical performance was investigated in two and three electrodes laboratory cells to differentiate polarization on the metal anode and organic cathode. Electrochemical mechanism of organic moiety during reversible Ca cation coordination was investigated through *ex situ* IR spectroscopy and energy dispersive spectroscopy (EDS) to determine the speciation of Ca cations (Ca^{2+} and $Ca[B(hfip)_4]^+$), which counterbalance the negative charge on the reduced anthraquinone groups.

2. Results and Discussion

The first and necessary requirement for the realization of the Ca metal-organic battery is efficient Ca electrolyte enabling Ca plating/stripping with the low overpotential and high reversibility. The synthesized $[Ca(dme)_4][B(hfip)_4]_2$ salt was carefully characterized with a multitude of analytical techniques in order to confirm salt purity and structure. ^1H and ^{13}C NMR show that stoichiometric quantities of $Ca(BH_4)_2 \cdot 2thf$ and hexafluoroisopropanol (hfipH) reacted completely and that no residual hfipH could be detected in the spectra (Figure S1). Both single-crystal and powder X-ray diffraction (XRD) (Table S1, Figure S2) of the salt are in a good agreement with the crystallographic data from the literature.[14,15] Attenuated total reflection infrared spectroscopy (ATR-IR) allowed the identification of several characteristic bands for the salt anion belonging to C–CF_3, B–O–C, two C–O stretchings and CF_3 deformation modes at 1381, 1187, 1097, 1053 and 686 cm^{-1}, respectively (Figure S3). All other salt characterization techniques are discussed in more detail in the SI and support the conclusion regarding the successful synthesis of $[Ca(dme)_4][B(hfip)_4]_2$ (Figure S4, Table S2).

Plating/stripping of Ca metal in the prepared electrolyte was assessed through cyclic voltammetry (CV) on a stainless steel electrode (Figure 1). As can be seen from the CV curves, there is an activation in the initial cycles, which is connected with the use of the 2-electrode electrochemical cell and the overpotential contribution from Ca counter electrode that has to be taken into account. Lack of additional anodic peaks shows that the electrolyte has good oxidative stability and should enable testing of the cathode materials in the voltage window up to 3.3 V vs. Ca metal reference. Coulombic efficiency of the Ca stripping increased from an initial 53% up to 67%, where it stabilized. The decrease in the Coulombic efficiency from literature reports[14,15] could be attributed to the use of the stainless steel working electrode, instead of noble-metal electrodes, and the change in the electrochemical setup. Deposition of Ca metal was confirmed through scanning electron microscopy (SEM) and EDS analysis of metal deposits

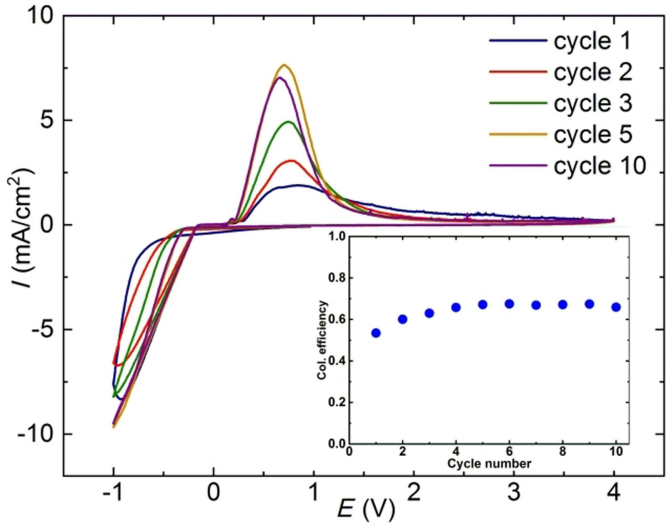

Figure 1. a) Selected cycles of cyclic voltammetry of 0.3 M $Ca[B(hfip)_4]_2$ in dme on stainless steel electrode in the voltage window from −1.0 to 4.0 V with a sweep rate of 25 mV/s. Inset is displaying Coulombic efficiency of Ca plating/stripping during the corresponding cyclic voltammetry test.

(Figure S5 and Table S3). Current efficiency of Ca plating/stripping is suitable for proof-of-concept testing on the lab scale, but in real cells, metal plating/stripping efficiencies higher than 99.9% are to be targeted. In our cell setup, non-uniform Ca metal deposition was observed, similar to the literature.[14,15]

After confirming the reversibility of the Ca plating/stripping process, the synthesized electrolyte was used to test the organic cathode. Anthraquinone-based polymer PAQS, having so far displayed reversible electrochemical activity in various metal electrolytes,[20,23,25] was chosen as a model organic electrode material. First tests with the plain polymer displayed low activity, with only approximately 20% of the theoretical capacity and with a relatively high polarization at a low current density of 0.2 C (Figure S6). To improve its performance, PAQS was polymerized in a suspension of multi-walled carbon nanotubes (CNTs), giving a nanostructured PAQS/CNTs composite that was used as an active material. SEM analysis (Figure 2a and b) shows that the polymer is well interconnected with the CNTs and displays a highly porous structure. The nanostructured cathode delivered a first discharge capacity of 169.3 mAh/g (Figure 2c), which is 75% of the theoretical one (225 mAh/g), confirming a significant improvement due to well established electronic wiring by using CNTs. Incorporation of CNTs induces a more porous structure of the polymer, which also improves ionic wiring within the active material. The discharge in the first plateau is different from the subsequent

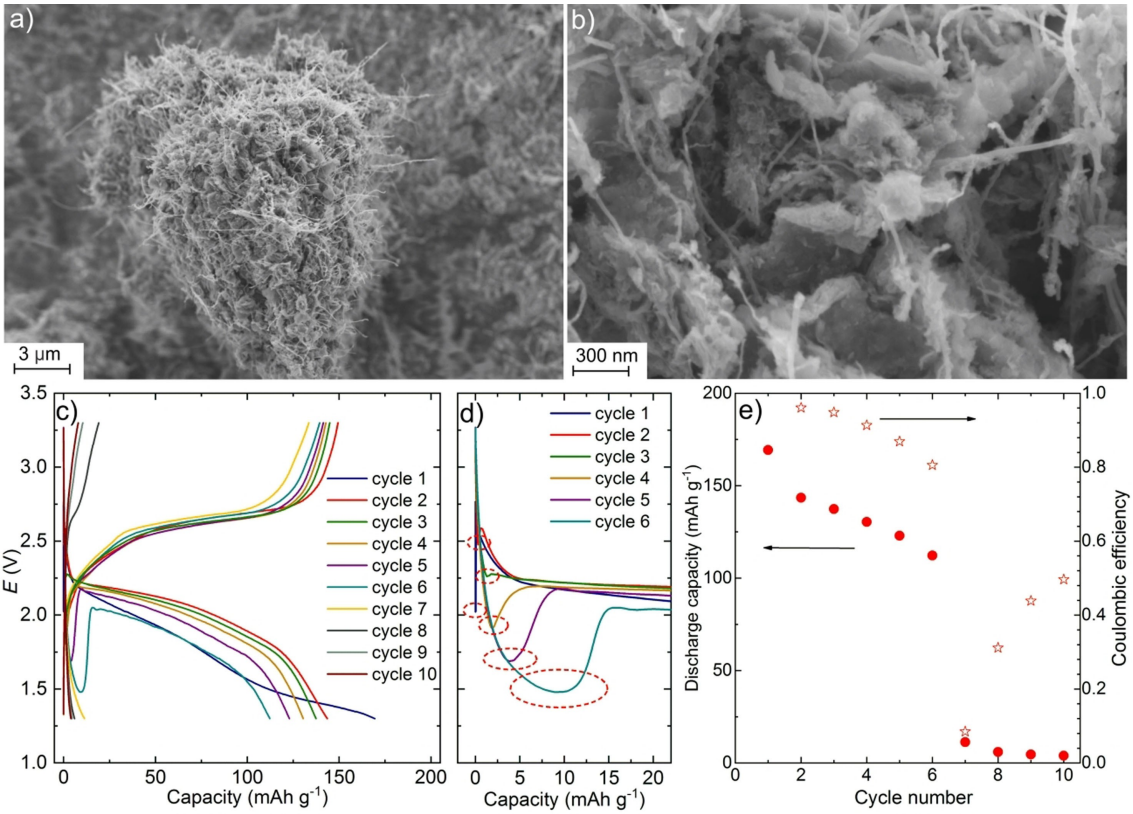

Figure 2. a) and b) Scanning electron micrographs of PAQS/CNTs composite at two different magnifications. c) Galvanostatic cycles of Ca metal-PAQS/CNTs battery cell at 0.5 C (122.5 mA/g) in the voltage range between 1.3 and 3.3 V. d) Inset into the start of the discharge curve for the first five cycles. The voltage axis is the same as on c) part of the figure, voltage dips are circled with the red dash circle. e) Corresponding discharge capacity and Coulombic efficiency for the Ca metal-PAQS/CNTs battery cell. Measurement was performed in the 2-electrode cell.

cycles, a feature previously observed in other electrolytes.[23,25] In the second cycle, the discharge plateau became less inclined, and it was upshifted to an average discharge voltage of 2.1 V. With further cycling, the polarization between discharge and charge curves started to increase and the average discharge plateau in the 5th cycle dropped to 1.9 V. In contrast, the increase of the overpotential is much smaller during charge. The increase of the overpotential is also accompanied by an increase of the voltage dip at the beginning of the discharge half-cycle (Figure 2d). At the start of the first discharge, there is only a short sharp peak, but this peak becomes both deeper and longer with cycling. This phenomenon can be assigned to the increase of the overpotential for Ca stripping at the Ca metal anode, which takes place during the discharge, as shown in Figure 3. Such an increase in the overpotential results in a significant decrease of the cathode capacity, from 169.3 mAh/g in the first cycle down to 112.3 mAh/g in the 6th cycle (Figure 2e). In the following cycles, the overpotential at the beginning of the discharge increased further and eventually led to the blocking behavior of the cell.

Tests in the three electrode laboratory cell setup with a Ca metal strip as a reference electrode were performed to confirm the hypothesis that the increased overpotential on the calcium anode led to the fast degradation of Ca metal-organic battery in two electrode laboratory cell setup. Figure 3 shows the electrochemical characterization of Ca metal-organic battery in the three electrode cell. The first important difference is the absence of a voltage dip at the beginning of the discharge in the half-cell between the working electrode (cathode) and the reference electrode (Figure 3a). The overpotential during the first discharge is related to the initial reduction process where pathways for transport of calcium cation need to be established. After the first discharge, the overpotential for discharge drops and well-defined plateau for anthraquinone redox reaction was obtained. Interestingly, even in the three electrode cell setup overpotential during discharge increases, while it remains stable during charge. As expected the shape of galvanostatic cycle does not change from 2- to 3-electrode cell and displays a single discharge plateau, which is better seen as a derivative of the galvanostatic curve (Figure S7) or CV performed in three electrode cell (Figure S8). This means that reduction of anthraquinone group proceeds as a one-step two-electron reduction or two-step one-electron reduction at relatively similar potential.[31] A big increase of the overpotential with cycling is observed between reference and counter electrode during the Ca stripping process (Figure 3b), and it is in a good agreement with results obtained in a two electrode cell. This has important implications for the energy efficiency of such cells since energy losses are increasing both through an increase of overpotential and increase of the time that this overpotential is present during the discharge of the full cell. After the initial peak, the overpotential for Ca stripping from Ca anode is around 0.05 V. The overpotential for Ca plating is several times larger, around −0.30 V versus the Ca metal potential and remains stable during cycling. After 10 cycles, a capacity of 114.2 mAh/g is obtained (Figure 3c), confirming that both the capacity fade at the cathode and the increase of the overpotential at the Ca anode are responsible for the fast capacity decay in the 2-electrode cell, with a larger contribution of the latter. Most likely, the increase of the overpotential at the Ca anode is connected with the accumulation of the degradation species from the electrolyte and deposition of the CaF_2 on the Ca metal anode. The formation of the CaF_2 along with the plating of Ca metal was already observed in the previous reports on the use of $Ca[B(hfip)_4]_2$ electrolyte.[14,15]

This demonstrates the feasibility of the Ca metal-organic battery as a sustainable alternative solution for energy storage. Theoretically, Ca metal-PAQS battery could offer an energy density of around 400 Wh/kg, while substitution of the relatively large anthraquinone group with the smaller and higher redox potential benzoquinone group could raise energy density of such cells up to 941 Wh/kg (calculations provided in the SI). Gravimetric energy density is comparable to the state-of-the-art Li-ion cells, while one can expect a decrease in the

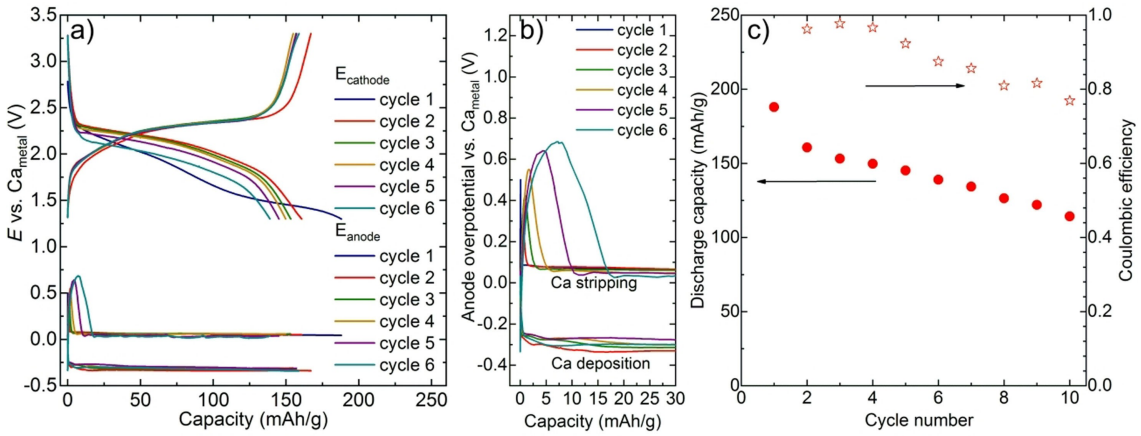

Figure 3. a) Galvanostatic cycling of Ca metal-PAQS/CNTs cell with Ca reference electrode at 0.5 C (122.5 mA/g). The top curves show the potential of PAQS/CNTs cathode, whereas the bottom curves show the potential of Ca metal anode. Part of Ca metal anode potential over 0 V corresponds to the Ca stripping process and part below 0 V to the Ca plating process. b) Inset into starting part of the overpotential on Ca metal in the magnified voltage range. c) Discharge capacity and Coulombic efficiency during cycling. Measurement was performed in the 3-electrode cell.

volumetric energy due to lower density of organic materials in comparison to inorganic ones.

Reversible electrochemical reaction of PAQS with the Ca ions can be confirmed by studying its reaction mechanism. In the case of the conjugated carbonyl compounds, we expect the reversible reduction of the carbonyl to the phenolate group with the addition of one electron per carbonyl group if full theoretical capacity is utilized (Figure 4a). This change can be followed by infrared spectroscopy, with the decrease in the intensity of the carbonyl band upon discharge and the simultaneous appearance of a new band representing the phenolate group.[32] To observe the PAQS electrochemical mechanism, three *ex situ* electrodes were prepared. One electrode was only soaked in the electrolyte and washed. The other two electrodes were cycled (one discharged, and the second discharged and recharged). Soaking of the electrode in the electrolyte did not cause any major changes (Figure 4b). Very low-intensity bands were observed in the region between 1100 and 1000 cm^{-1}, which could be attributed to traces of the electrolyte and could be assigned to C–O stretching modes. The spectrum of the discharged electrode displayed the completely different bands and looked relatively noisy. The C=O double band at 1674 and 1650 cm^{-1}, the –C=C– stretching at 1570 cm^{-1} and the C–H out of plane bending at 704 cm^{-1}, which are characteristic of the PAQS polymer, disappeared, while a new band at 1374 cm^{-1} was observed, which can be assigned to the phenolate groups and is consistent with previous observations in the reduced monovalent (Li)[32] and bivalent (Mg)[33] anthraquinone salts. Even though this band is relatively broad and is close to the C–CF_3 stretching band belonging to the salt anion, its observed downshift indicates that both vibrational modes contribute to this band. Several additional bands in the region between 1200 and 1000 cm^{-1} were observed, together with a very intense C–F vibration band at 686 cm^{-1} that can be confused for downshifted C–H out of the plane vibration. The existence of these bands in the discharged cathode spectra indicates the presence of the $[B(hfip)_4]^-$ anion in the discharged cathode or formation of the cathode electrolyte interface from the decomposed salt (Figure S9). The charged cathode again displays well-defined C=O and C–C stretching bands together with the C–H out of plane vibration, indicating good reversibility of the electroactive carbonyl groups. The remainder of the stretching bands between 1200 and 1000 cm^{-1} and C–F vibration band in the charged cathode indicate incomplete charging (88% according to the capacity difference between discharge and charge) or the possible presence of electrolyte decomposition products.

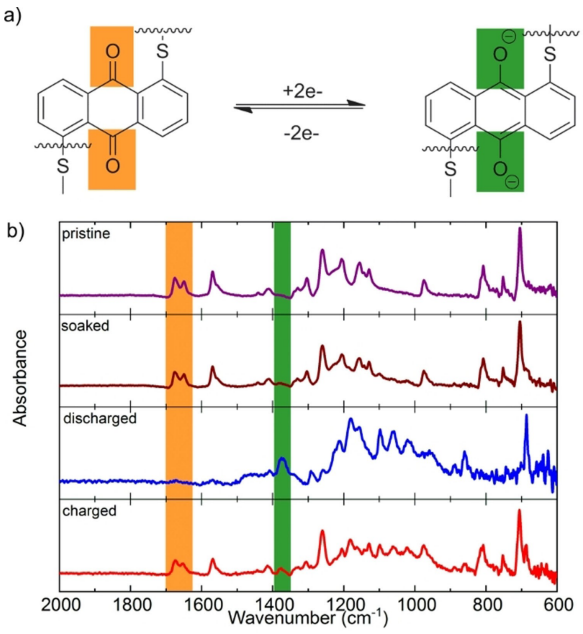

Figure 4. a) Electrochemical reaction of PAQS electrochemical group upon cell discharge. b) ATR-IR spectra of *ex situ* PAQS/CNTs electrodes. Pristine electrode (purple), electrode soaked in the electrolyte and washed (brown), discharged electrode (blue) and charged electrode (red). The areas of the highest interest are shaded. Corresponding electrochemical data for discharged and charged electrode are presented in Figure S9.

Enabling Ca^{2+} storage is of the utmost importance to achieve high energy Ca metal-organic batteries, and the presence of monovalent cations ($Ca[B(hfip)_4]^+$) as counter ions to the quinone groups in the reduced state would greatly decrease the energy density of this system and prevent cell operation in the lean electrolyte conditions.[25,34] SEM EDS was thus used to check the possible presence of $[B(hfip)_4]^-$ in the discharged compound (Table 1). From the mass of the discharged electrode (see SI for details about the calculation), it could be concluded that the mass increase of 77% cannot be explained by coordination of $PAQS^{2-}$ with Ca^{2+} nor with $Ca[B(hfip)_4]^+$ cations. The former would, upon 100% PAQS capacity utilization, mean a mass increase of about 9%, while the latter would mean an increase of mass of 326% due to the presence of two bulky $Ca[B(hfip)_4]^+$ anion-paired cations. Thus, the most probable scenario is that majority of charge is compensated by Ca^{2+} with a much smaller contribution of $Ca[B(hfip)_4]^+$. The ratio of $Ca[B(hfip)_4]^+$ cation that is used for

Table 1. Atomic ratios of elements present in the electrodes, normalized per S content. In the last column, relative increase of the mass for specific electrodes is reported.

Electrode	C	O	F	F active[a]	S	Cl	Ca	Mass increase [%]
Pristine & soaked	35.72	2.88	3.61	0	1.00	0.16	0.03	3
Discharged	42.62	6.98	13.99	10.38	1.00	0.17	1.03	77
Charged	36.15	2.43	4.63	1.02	1.00	0.15	0.13	12

[a] Additional column F active is introduced to differentiate between non-active F, which was present as PTFE binder and should remain constant through the electrochemical cycling, and active F, which was part of $[B(hfip)_4]^-$ anion. F active was calculated after F content in the pristine & soaked electrode was subtracted from the discharged and charged electrode. More details about the calculations are available in the Supporting Information.

coordination of reduced quinone group can be estimated from the increase in F content in the electrode in the discharged state. From F active (not belonging to PTFE binder) and Ca content (24 F atoms per $Ca[B(hfip)_4]^+$ cation), speciation of PAQS can be estimated and calculation yields 57% $PAQS^{2-}$–Ca^{2+}, 21.5% $PAQS^{2-}$–$2Ca[B(hfip)_4]^+$, and 21.5% undischarged PAQS in molar percentage. From this assessment, a discharged capacity of 177 mAh/g (172 mAh/g measured) and a mass increase of 75% (77% measured) can be estimated, which is in a good agreement with the measured values. Although a non-negligible fraction of the $Ca[B(hfip)_4]^+$ ion-paired cations definitely takes part in the electrochemical reaction, most of the charge is still compensated by the lean Ca^{2+} cations. EDS characterization of the charged electrode shows that incomplete charge (88% according to capacities in Figure S10) still has an increased F active and Ca content in the electrode. Given the similar ratios between F and Ca in discharged and charged electrode, the preferential charging of the PAQS cathode can be excluded.

While this study demonstrates the feasibility of a Ca-organic battery working at room temperature, opening a sustainable direction for rechargeable Ca batteries, at the same time it also demonstrates the need for further development and optimization of Ca electrolytes with anions that can weakly coordinate divalent cations. Properly designed electrolytes having high reductive stability, good efficiency for Ca plating/stripping process and high dissociation constant for Ca salt are required for practically viable Ca batteries, including the Ca-organic battery studied in this work.

3. Conclusions

The recent development of novel Ca electrolytes has enabled Ca plating/stripping at room temperature. However, the development of Ca cathode materials is still lagging behind and is hindering the development of practical Ca rechargeable batteries. Herein, a proof-of-concept Ca metal-organic battery was demonstrated through the application of organic polymer cathode. Good reversibility of Ca^{2+} insertion at the cathode was established, but after a few reversible cycles in a 2-electrode cell setup, a big increase in the overpotential resulted in a sudden drop of the cell capacity. Application of the 3-electrode cell allowed us to pinpoint this overpotential to Ca metal anode during the Ca stripping process. Reversibility of anthraquinone-based cathode confirmed through *ex situ* ATR-IR, displaying a reversible reduction of carbonyl bond upon discharge. The reduction of the carbonyl bond was compensated mainly by the coordination with Ca^{2+} and in smaller part (less than 30%) also by $Ca[B(hfip)_4]^+$ monovalent cation, as confirmed by *ex situ* EDS analyses. These results demonstrate the practical applicability of Ca metal-organic batteries and provide a very good starting point for the future development of organic electrodes for Ca batteries through demonstration of strengths and weaknesses of the current setup. After all, coordinated development of both cathode and electrolyte will be needed to achieve high reversibility of Ca metal plating/stripping, to enable facile dissociation of the calcium salts, and to improve cathode capacity retention.

Acknowledgements

A.S. acknowledges ALISTORE-ERI for his PhD grant. The authors would like to acknowledge financial support from Slovenian Research Agency under research projects Z2-1864, J1-1705 and research programs P2-0393, P1-0230, P1-0045 as well as French National Research Agency (ANR) under the public grant ANR-10-LABX-76-01 (Labex STOREX) as part of the "Investissements d'Avenir" program. The authors thank Edi Kranjc from National Institute of Chemistry for the capillary salt powder XRD acquisition and EN-FIST Centre of Excellence for use of the SuperNova diffractometer.

Conflict of Interest

The authors declare no conflict of interest.

Keywords: calcium metal battery · organic cathode · calcium tetrakis(hexafluoroisopropyl)borate · electrochemical mechanism · anthraquinone

[1] J.-M. Tarascon, *Nat. Chem.* **2010**, *2*, 510.
[2] H. Kawamoto, W. Tamaki, *Sci. Technol. Trends, Quart. Rev.* **2011**, *39*, 51–64.
[3] M. M. Thackeray, C. Wolverton, E. D. Isaacs, *Energy Environ. Sci.* **2012**, *5*, 7854–7863.
[4] D. Larcher, J.-M. Tarascon, *Nat. Chem.* **2015**, *7*, 19–29.
[5] A. Ponrouch, J. Bitenc, R. Dominko, N. Lindahl, P. Johansson, M. R. Palacin, *Energy Storage Mater.* **2019**, *20*, 253–262.
[6] M. Jäckle, K. Helmbrecht, M. Smits, D. Stottmeister, A. Groß, *Energy Environ. Sci.* **2018**, *11*, 3400–3407.
[7] M. Matsui, *J. Power Sources* **2011**, *196*, 7048–7055.
[8] D. Aurbach, R. Skaletsky, Y. Gofer, *J. Electrochem. Soc.* **1991**, *138*, 3536–3545.
[9] M. E. Arroyo-de Dompablo, A. Ponrouch, P. Johansson, M. R. Palacín, *Chem. Rev.* **2020**, 120, 6331–6357, DOI 10.1021/acs.chemrev.9b00339.
[10] R. J. Staniewicz, *J. Electrochem. Soc.* **1980**, *127*, 782–789.
[11] A. Meitav, E. Peled, *J. Electrochem. Soc.* **1982**, *129*, 451-457.
[12] A. Ponrouch, C. Frontera, F. Bardé, M. R. Palacín, *Nat. Mater.* **2016**, *15*, 169–172.
[13] D. Wang, X. Gao, Y. Chen, L. Jin, C. Kuss, P. G. Bruce, *Nat. Mater.* **2018**, *17*, 16–20.
[14] Z. Li, O. Fuhr, M. Fichtner, Z. Zhao-Karger, *Energy Environ. Sci.* **2019**, *12*, 3496–3501.
[15] A. Shyamsunder, L. E. Blanc, A. Assoud, L. F. Nazar, *ACS Energy Lett.* **2019**, *4*, 2271–2276.
[16] D. S. Tchitchekova, C. Frontera, A. Ponrouch, C. Krich, F. Bardé, M. R. Palacín, *Dalton Trans.* **2018**, *47*, 11298–11302.
[17] D. S. Tchitchekova, A. Ponrouch, R. Verrelli, T. Broux, C. Frontera, A. Sorrentino, F. Bardé, N. Biskup, M. E. Arroyo-de Dompablo, M. R. Palacín, *Chem. Mater.* **2018**, *30*, 847–856.
[18] A. L. Lipson, S.-D. Han, S. Kim, B. Pan, N. Sa, C. Liao, T. T. Fister, A. K. Burrell, J. T. Vaughey, B. J. Ingram, *J. Power Sources* **2016**, *325*, 646–652.
[19] C. R. DeBlase, K. Hernández-Burgos, J. M. Rotter, D. J. Fortman, D. dos S. Abreu, R. A. Timm, I. C. N. Diógenes, L. T. Kubota, H. D. Abruña, W. R. Dichtel, *Angew. Chem. Int. Ed.* **2015**, *54*, 13225–13229; *Angew. Chem.* **2015**, *127*, 13423–13427.
[20] Z. Song, H. Zhan, Y. Zhou, *Chem. Commun.* **2009**, 448–450.
[21] C. Guo, K. Zhang, Q. Zhao, L. Pei, J. Chen, *Chem. Commun.* **2015**, *51*, 10244–10247.

[22] Z. Jian, Y. Liang, I. A. Rodríguez-Pérez, Y. Yao, X. Ji, *Electrochem. Commun.* **2016**, *71*, 5–8.
[23] J. Bitenc, K. Pirnat, T. Bančič, M. Gaberšček, B. Genorio, A. Randon-Vitanova, R. Dominko, *ChemSusChem* **2015**, *8*, 4128–4132.
[24] B. Häupler, C. Rössel, A. M. Schwenke, J. Winsberg, D. Schmidt, A. Wild, U. S. Schubert, *NPG Asia Mater.* **2016**, *8*, e283.
[25] J. Bitenc, N. Lindahl, A. Vizintin, M. E. Abdelhamid, R. Dominko, P. Johansson, *Energy Storage Mater.* **2020**, *24*, 379–383.
[26] T. B. Schon, B. T. McAllister, P.-F. Li, D. S. Seferos, *Chem. Soc. Rev.* **2016**, *45*, 6345–6404.
[27] J. Bitenc, K. Pirnat, E. Žagar, A. Randon-Vitanova, R. Dominko, *J. Power Sources* **2019**, *430*, 90–94.
[28] Z. Song, Y. Qian, M. L. Gordin, D. Tang, T. Xu, M. Otani, H. Zhan, H. Zhou, D. Wang, *Angew. Chem.* **2015**, *127*, 14153–14157; *Angew. Chem. Int. Ed.* **2015**, *54*, 13947–13951.
[29] I. A. Rodríguez-Pérez, Y. Yuan, C. Bommier, X. Wang, L. Ma, D. P. Leonard, M. M. Lerner, R. G. Carter, T. Wu, P. A. Greaney, J. Lu, X. Ji, *J. Am. Chem. Soc.* **2017**, *139*, 13031–13037.
[30] S. Gheytani, Y. Liang, F. Wu, Y. Jing, H. Dong, K. K. Rao, X. Chi, F. Fang, Y. Yao, *Adv. Sci.* **2017**, *4*, 1700465. .
[31] J. Bitenc, A. Vizintin, J. Grdadolnik, R. Dominko, *Energy Storage Mater.* **2019**, *21*, 347–353.
[32] A. Vizintin, J. Bitenc, A. Kopač Lautar, K. Pirnat, J. Grdadolnik, J. Stare, A. Randon-Vitanova, R. Dominko, *Nat. Commun.* **2018**, *9*, 661.
[33] J. Bitenc, T. Pavčnik, U. Košir, K. Pirnat, *Materials* **2020**, *13*, 506.
[34] H. Dong, Y. Liang, O. Tutusaus, R. Mohtadi, Y. Zhang, F. Hao, Y. Yao, *Joule* **2019**, 3, 782–793. .

Manuscript received: August 21, 2020
Revised manuscript received: September 14, 2020
Accepted manuscript online: September 14, 2020
Version of record online: October 13, 2020